CHAPTER 4

GRAPHITE

The graphitisation process is essentially an ordering of the carbon atoms within the carbon matrix towards the perfect structure of hexagonal graphite in a heat-treated carbon. The quality of the graphite depends on the purity and quality of the starting material, and its specific properties depend on its end use. The transition to graphite is not only temperature-dependent or time-dependent, it is a factor of the additives used in the starting material. However, the kinetics of the graphitisation process do not form part of this discussion. Graphite is not composed entirely of carbon but also contains heteroatoms such as H, N and O, etc. The effect of these heteroatoms on graphitisation will therefore also be examined. Understanding the effect of additives in modifying the graphite's properties and in lowering the temperature required to bring about a certain degree of graphitisation or to promote a more graphitic structure are important objectives of this chapter.

4.1 Crystalline forms of carbon

The two known crystalline forms of carbon are diamond and graphite. Diamond is a metastable crystalline form of carbon, with a face-centred cubic lattice of side 3.5667 Å and can be converted to graphite by heating. The carbon atoms are bonded tetrahedrally to four other carbon atoms. To convert graphites to diamond requires both elevated temperatures and pressures. The structure of graphite as reported by Warburton was first proposed by Hull (1917) and confirmed by Bernal (l924) [67]. The structure has a hexagonal unit cell of dimensions $L_a = 2.4615$ Å and $L_c = 6.708$ Å, and an interlayer spacing (d_{002}) of 3.354 Å. The atoms are hexagonally arranged in layers, with the interatomic

distance being 1.42 Å [144]. The layers are arranged in a regular starting sequence ABABAB (see Fig. 4.1).

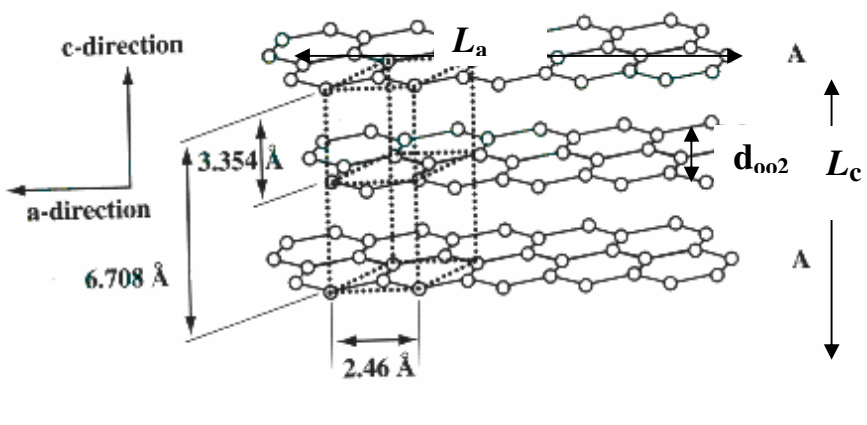

Figure 4.1: The structure of graphite [140]

The structure of graphite does *not* show certain faint lines in the X-ray diffraction powder photographs of both natural and artificial graphites as was thought earlier from electron diffraction photographs of graphite [145, 146]. Instead, the lines found were due to the presence of a rhombohedral structure (about 14 %) in which the layers were stacked ABCABC (Fig. 4.2b) [67].

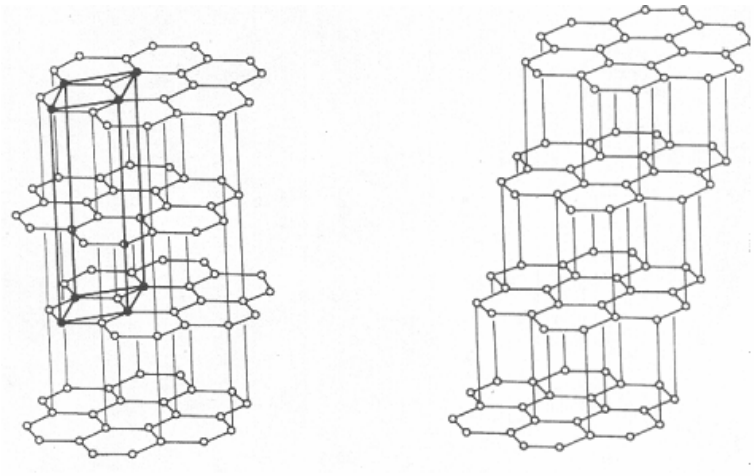

Hexagonal (a) Rhombohedral (b)

Figure 4.2: Lattice structure of hexagonal (with unit cell) and Rhombohedral structures in graphite [67].

It was further proposed that the rhombohedral form comprised up to 30 % of natural graphite and that it could be converted to the hexagonal form (Fig. 4.2a) by heating to 2 000 ~ 3 000 ^{o}C. Because the rhombohedral form has never been isolated, doubt has arisen as to whether it is a separate crystalline form or simply a stacking fault in the hexagonal ABABAB sequence, producing ABCABC sequences. The enthalpy change in going from rhombohedral to hexagonal graphite was reported to be - 0.l44 ± 0.041 kcal per g-atom (- 602.496 ± 171.544 J per g-atom), thus confirming that hexagonal graphite is the most stable phase [147].

4.2 The graphitisation process

Graphitisation as reported by Warburton in the work of Houska and Warren (1954) was based on an incorrect structural model. Small layers in carbon black were thought to grow (either by migration of individual atoms from one layer to another, or by joining of layers) to reach a size (L_a = 100 Å) that was energetically favourable for pairs of nearest neighbours to rotate and take on the graphite relationship [148]. However, the model has been superseded by one in which large layers are already present, the graphitisation process being the thermal annealing out of the defects at low temperature.

Despite the lack of a satisfactory model for pre-graphite carbon, there was enough evidence that such carbons contain extensive areas of graphite-like material. The mesophase studies of Brooks and Taylor [74] demonstrated how this came about. These extensive graphite-like layers are imperfect, although the nature of the imperfection is open to discussion. Whatever their nature, the removal of these imperfections by heating to elevated temperature is responsible for bringing about the formation of a graphitic carbon.

Graphitisation is entirely different from the process just described. Firstly, it takes place in hard carbons and secondly, it involves only a small percentage of the carbon atoms present [149]. Many non-graphitising carbons when heated to temperatures between 2 000 and 3 000 ^{o}C were found to contain a small proportion of graphitic carbon. This was detectable from the diffuse (002) band superimposed upon it, either one (2-phase graphitisation) or two (3-phase graphitisation) sharp lines [150]. The conclusion drawn was that these graphitic components were caused by the high internal stresses set up during thermal treatment. It was thought that a localised crystallisation, under high pressure, had taken place in the interior of the solid. This formation of graphitic carbon would relieve the stress in the remaining cross-linked structure and when the tension in the non-graphitic structure had been reduced sufficiently, the formation of graphitic carbon ceased. Franklin's rigid classification into graphitising and non–graphitising carbons [149] is no longer valid and two–phase graphitisation could take place in what was termed 'non-graphitising carbons' (e.g. epoxide resins, phenol–formaldehyde resins, intermediate carbons (3,5-xylenol/formaldehyde) and in 'graphitising' carbons (polyvinyl acetate, Ford's pitch) [151]. The temperatures at which the graphitic components first appeared were, however, very different. The components appeared in the graphitising carbons at less than 1 000 ^{o}C, at between 1 000 and 2 000 ^{o}C for the intermediate carbons, but not until 2 000-2 600 ^{o}C for the non-graphitising carbons. The non-graphitic component was thought to be due to non-organised carbon. The latter view is somewhat surprising as it is reported that non-organised carbon is present in all the graphitising carbons examined, even at 2 600 ^{o}C.

4.3 The effect of heteroatoms and/or additives

The incorporation of elements such as boron, nitrogen, oxygen and sulphur into the layer planes of a pre-graphitic carbon is analogous to their existence in heterocyclic ring compounds. It has been reported that 1 - 2 atoms of boron could be stably incorporated into the graphite. Carbon prepared at 1 000 ^{o}C or

below may contain up to several per cent by weight of heteroatoms [152]. The majority of heteroatoms are, however, removed by heating to temperatures in excess of 1 500 ^{o}C. It was found that the hydrogen content of the various cokes studied was less than 0.1 ppm at 1 500 ^{o}C, but 40 - 50 ppm of hydrogen persisted in commercial-grade nuclear graphite which had been heated to about 2 700 ^{o}C . About 200 ppm of sulphur in commercial graphite is retained up to temperatures much higher than 2 000 ^{o}C [152].

Small amounts of oxygen in the atmosphere of a baking furnace were found to increase the yield of coke from the binder and thus increase the strength of the artefact [153]. The oxygen acted presumably by forming cross-linkages.

Dehydrochlorination of polyvinyl chloride in the presence of air, at temperatures below 250 ^{o}C, formed non–graphitising carbon, whereas heating in an inert atmosphere produced graphitising carbon [154]. The exposure to air was thought to produce extensive cross-linkages, which inhibited the fusion that may otherwise have occurred in the later stages of carbonisation. It has been noted that for many carbons (e.g. polyvinyl chloride, sucrose and a variety of industrial cokes), the temperature at which the concentration of heteroatoms dropped to less than 0,1 % was close to that at which the three–dimensional ordering commenced [154].

It has been reported that treatment of fibres prepared from molten polyvinyl chloride in ozone and oxygen resulted in an infusible and completely insoluble product (in all solvents) [155, 156]. It was concluded this was due to the formation of cross-linkages between the aromatic planes. Kipling *et al*. [54, 154] found that the progressive addition, prior to carbonisation, of sulphur to polyvinyl chloride led to reduced graphitisability. The addition of 9 % sulphur was thought to be sufficient to change a polyvinyl chloride carbon, heat-treated at 2 700 ^{o}C, from graphitic to non-graphitic carbon. Microscopic examination showed that in

the intermediate range of sulphur addition (5% S), there was a two–phase structure – one phase graphitic, the other non-graphitic.

The conclusion reached was that sulphur acted by forming cross-linkages and promoting dehydrogenation. It is interesting to compare the results of Kipling *et al.* [54, 154] with those of Ihnatowicz *et al.* [95] who studied the effect of oxygen content on the formation of the mesophase spheres. These results showed that for an oxygen content of greater than 7 %, no spheres were formed; from 5 - 7 % oxygen, only small isolated spheres were formed; and only those carbons that originally contained less than 5 % oxygen showed extensive formation of spheres. It would appear from this work that there is a minimum amount of oxygen or sulphur tolerated: up to 7 % oxygen and 9 % sulphur [157].

However, Gillot *et al.* found that removing the sulphur (by heating with hydrogen) from a petroleum coke, at a temperature lower than that at which it would normally be removed, led to the formation of a small fraction of graphitic carbon (d = 3,36 Å, L approx. 500 Å) [158]. A linear relationship was found to exist between the square root of the concentration of heteroatoms and the graphitisability of carbons derived from Catarex pitch, although the addition of sulphur (up to 16.7 % in the case of acenaphthylene) to diphenylamine and acenaphthylene, prior to carbonisation, did not produce any change in their graphitisability [159, 160].

4.4 Catalytic graphitisation

Since the graphitisation process is essentially an ordering of carbon atoms within the carbon matrix towards the perfect structure of hexagonal graphite, heat treatment to temperatures around 3 000 ^{o}C can produce these changes, with the vibrational energy of the lattice being increased sufficiently to promote the atomic displacements. Heat treatment, however, is not the only experimental parameter available to bring about changes. The addition of certain inorganic and organic

additives can improve the graphitisation process. The overall effect is to lower the temperature required to bring about a certain degree of graphitisation or to promote a more graphitic structure at a fixed heat-treatment temperature.

4.4.1 Mechanisms of catalytic graphitisation

The mechanism of catalytic graphitisation varies from system to system, and depends upon the additive and the nature of the carbon (hard or soft). Several distinguishable mechanisms in which the inorganic additives promote graphitisation have been reported. The more familiar mechanism involves growing crystals of graphite from melts of either metal or metal carbide. These crystals dissolve the carbon into amorphous carbon and reprecipitate it as graphite either when it is cooled or as a natural consequence of supersaturation. The driving force of the reaction is a favourable change in free energy in going from the disordered amorphous carbon to a highly ordered graphitic carbon. The production of Kish in the steel-making industry is a common example of this mechanism [161, 162].

In the other mechanism, elements such as aluminium, iron, silicon, etc. are thought to combine with carbon to form carbides. These carbides show appreciable thermal stability, as opposed to cobalt and nickel whose carbides decompose below 400 ^{o}C. The thermally stable metal carbides decompose around 1 500 ^{o}C or higher, and the carbide lattice leaves behind a graphitic lattice. Externally, these graphite crystals are pseudomorphs of the original carbide crystal and result from the vaporisation of the metal. A simple physical picture explaining this phenomenon may be that because these carbides are usually interstitial carbides, they contain close-packed layers of meta-atoms, between which lie the carbon atoms arranged in hexagons. When the metal leaves the lattice, the carbon atoms are left approximately in layers and within these layers they are arranged hexagonally. It is therefore easy to conceive a rearrangement to give the layered graphite structure [67].

4.4.2 The effect of additives on catalytic graphitisation

The incorporation of small amounts of non-volatile metallic oxides of aluminium, iron, magnesium, titanium or vanadium with pitch and binder is believed to catalyse the transition of the carbon to graphite [163]. Highly pure graphite was produced by the addition of aluminium carbide (Al_4C_3) and subsequently heating to 1100 ^oC in a stream of chlorine [164]. The carbide decomposed to graphite and acted as a nucleus for further graphitisation, and the metal was removed as volatile chloride. The temperature of 1 100 ^oC was lower than the decomposition temperature of the carbides (SiC, Fe_3C). Further heating to 2 000 ^oC for 2 h completed the graphitisation. The addition of Al_4C_3 led to an increase in the crystallite dimension L_c with a subsequent increase in the density of the graphite and an improvement in its neutron radiation stability.

In a heated series of metal compounds mixed with hard carbons at temperatures between 1 400 and 2 300 ^oC, X-ray diffraction techniques revealed aluminium to be an effective catalyst at 1 500 ^oC. An extra diffraction line was found and appeared to be due to an intermediate between the metal being considered and carbon. The decomposition of the intermediate is thought to have enhanced graphitisation [67].

The iron-carbon system in graphitisation has been well studied. Studies have focused primarily on the mechanism associated with carbon dissolving in molten iron and precipitation of the graphite. The intermediate carbide is formed. A large single crystal of graphite was grown by saturating solutions of iron (or nickel) with a low supersaturation of carbon, and then slowly cooling in steady-state thermal current [165]. However, the technique was later modified by dissolving the carbon in molten iron and evaporating the iron at an elevated temperature. The iron enclosed in the graphite was evaporated at temperatures of 3000 – 3200 ^oC for an hour, resulting in the formation of graphite crystals from the central volume occupied previously by the evaporated iron [165].

The role of iron in the graphitisation of petroleum coke and of non-graphitising carbon from sucrose on heat treatment from 1 800 – 2 400 ^{o}C was studied. The results were postulated to follow the mechanism in which the iron combines with carbon to form cementite, which then decomposes into graphite. In the process, the iron diffused through the grains of the coke and altered the structure within the grains to promote graphitisation within the non-graphitising carbon [166].

Heating a hard carbon in the presence of iron transformed it into a mixture of graphite and graphitisable carbon. Observation of the external surfaces of the coke grains showed that they were not changed by the iron, although they appeared earlier – at 1 600 ^{o}C instead of 2 200 ^{o}C. The effect was observed within the grains of the coke: iron carbide or cementite appeared to have been formed within the boundaries of the domains constituting hard carbon. These domains became free to orientate themselves on the surface of the droplets of the iron carbide, with their carbon layers parallel to the surface. The droplets coalesced into graphitisable carbon. This means that graphite was produced by dissolution of iron to form Fe_3C and that carbon was precipitated as graphite [167].

Heat treatment of iron or iron compounds with amorphous carbon led to the formation of the carbide, cementite (Fe_3C), which decomposed on further heating to give graphite [168]. Dispersion of cementite in amorphous carbon at 110 ^{o}C over a stream of chlorine was found to decompose the carbide into graphite, which then nucleated the graphitisation at 2 000 ^{o}C for 2 h [164]. The formation of cementite as intermediate carbide was further reported to yield even better graphite when used in conjunction with silicon as ferrosilicon [169]. Improved graphite density and neutron stability was achieved on addition of ferric oxide and led to an increase in the crystallite size parameter L_c [170]. Incorporation of small amounts of iron oxide with pitch and coke was reported to enhance the transition from amorphous carbon to graphite [67, 159].

It can be concluded that iron or an iron compound catalysed the conversion of hard carbon into a graphitisable carbon by firstly dissolving the hard carbon to form an intermediate phase, cementite Fe_3C, which separated on further heating into graphite formed in the spaces left by the evaporated iron.

4.4.3 The effect of side-chains on graphitisation

Graphitisation of a series of carbazole derivatives substituted at the ring position by one or more methyl, ethyl or butyl group(s) revealed that these carbons become more graphitic with increased alkyl substitution and with increased chain size of the alkyl group [166]. Carbazoles normally form non-graphitisable carbons due to the radicals formed during carbonisation being non-planar and forming a three-dimensional cross-linked carbon. It was then postulated that the enhancement of graphitisation by alkyl substitution was most likely due to planar aromatic free radicals being formed by thermal cleavage of the alkyl group. A competing reaction by which carbazoles carbonised in the normal way occurred. Such competing reactions were thought to be responsible for the resulting multi-phase carbons. The extent of planar free radical formation was thought to be dependent on the number of alkyl groups per molecule and the case of formation of the radical [171].

In conclusion, it would appear that the inclusion of heteroatoms into the carbon precursor leads to a less graphitic product and this is exactly what would be predicted from the modern ideas on pre-graphitic carbons. The inclusion of a heteroatom must lead to the formation of a point defect, and the removal of defects of one sort or another is the very essence of what is now understood by the graphitisation process. An exception to the general rule, whereby carbonising in oxygen leads to a less graphitic product, has, however, been reported. A more graphitic carbon was derived from a poly-2-h-dimethylphenylene oxide which had been cross-linked, by pre-oxidation, before pyrolysis [172]. It was shown that

after such a carbon had been heated to 2 900 ^{o}C, the d-spacing was 3.36 Å compared with 3.38 Å for the non-oxidised polymer, despite the fact that the polymer was known to exhibit melting during the first stage of pyrolysis. The reason for this anomaly is that the ether bridge in the un-oxidised polymer is ruptured at 370 ^{o}C, producing a rigid system of benzene rings separated by a conjugated system of one single and one double bond.

Condensation of this polymer occurred at 400 ^{o}C to produce an aromatic system that was incapable of building up into an extended aromatic layer without the inclusion of vacancies. The ether bridges in the oxidised polymer, on the other hand, rupture at temperatures ranging from 300 – 500 ^{o}C and continuous rearrangement of the intermediates created an aromatic system that was capable of producing an extended aromatic layer [172].

The above studies all relate to heteroatoms incorporated during carbonisation, either by exposure to air or by addition prior to carbonisation. Further study of carbonisation on aromatic hydrocarbons with heteroatoms revealed that not all of these molecular species form non-graphitising carbons. It appeared that if a compound forms an intermediate, with the elimination a heteroatom, the intermediate condenses to form an extended aromatic molecule, resulting in good graphitisability. Heterocyclic compounds containing sulphur and nitrogen could produce quality graphite [173].

Oxygen, sulphur or nitrogen, when present in the precursor, remains entrapped in the carbon skeleton to 2 000 – 2 200 ^{o}C. The presence of these elements may result in the degradation of the aromatic ring system through the elimination of carbon dioxide. This degradation generally led to non-planar free radicals, which polymerised to give mostly a cross-linked disordered carbon. The enhancement of graphitisation by alkyl substitution was shown to be due to planar aromatic free radicals being formed by thermal cleavage of the alkyl group. The extent of planar free radical formation was dependent on the number of alkyl groups per

molecule and the manner of formation of the radical. Aromatic systems promote mesophase formation by virtue of their planarity and low reactivity [173, 174].

4.5 Properties of graphite important to the nuclear industry

This sub-section focuses on those applications of graphitisable carbon relevant to the nuclear industry. Its commercial use in aluminium as graphite electrodes, in steel as coke (as a reducing agent), as carbon mesophase powder for providing structural stability, as a lubricant and in aerospace as coke, though important, will not be discussed in this sub-section. The properties of graphite required for the reactor reflector in nuclear energy industry will be discussed.

Gilsonite material has been used in the United Kingdom and elsewhere as a starting material for the moderator graphite since it produces graphite with near-isotropic bulk properties. The coefficients of thermal expansion for an extruded Gilsonite pitch graphite are parallel and perpendicular to the extrusion direction, being 4.0 and 4.5 x 10^{-6} $^{o}C^{-1}$ respectively, whereas for an extruded petroleum coke graphite they are 1.3 and 3.2 x 10^{-6} $^{o}C^{-1}$ respectively [10]. Graphite forms a major component of the fuel, which is composed of particles of UO_2 kernels successively coated with pyrolytic carbon, silicon carbide and pyrolytic carbon. Graphites subjected to a high dosage of neutron irradiation (>5 x 10^{21}n/cm$^{2)}$ at 300 – 1 500 ^{o}C showed pores and cracks at the boundaries between the filler the particles, causing them to disintegrate. The effect was observed to be less marked for graphite with near-isotropic bulk properties than for conventional anisotropic graphites, when compared at the same neutron dosage and temperatures [11, 12].

A highly anisotropic coke leads to graphite with properties such as high magnetic susceptibility, high electrical conductivity and a high coefficient of thermal expansion. The strength of graphite at high temperature and its behaviour with respect to the products of nuclear fission/fusion make the material suitable as a

nuclear moderator and reflector, and as a material for construction and for thermal columns in various reactors [175]. Advanced gas-cooled reactors, high-temperature gas-cooled reactors, molten salt breeder reactors and liquid-fuelled reactors all use graphite moderators. Graphite suitable for nuclear reactors must have uniform coefficients of thermal expansion across and along the plane (a-axis and c-axis plane of the crystallite) so as to prevent the reactor block from swelling (see Table 4.1). (Isotropy of the graphite with low boron content is preferred as it confers the required properties on the graphite.)

Table 4.1: Properties of nuclear graphites [176]

Property	**Anisotropic graphite**	**Isotropic graphite**
Density (g/cm^3)	1.71	1.86
Resistance (μΩ·cm)	735	1 000
Tensile strength (kPa^c)	9.93	46.172
Coefficient of thermal expansion (10^{-6}/ ^{o}C)		
With grain	2.2	5.3
Against grain	2.8	5.3
Anisotropy ratio	1.73	1.0
Total ash (ppm)	740	400
Boron content (ppm)	0.4	0.3

The properties of two types of graphite used as moderators or reflectors in nuclear reactors are listed in Table 4.1. The data for the coefficient of thermal expansion indicate that anisotropic graphite shows unequal coefficients of thermal expansion in the a-axis and c-axis of the crystallite graphite and it is therefore not preferred for nuclear reactors [176].

With exposure to high-temperature radiation over a long time, graphite undergoes dimensional changes in length and volume. Fig. 4.3a shows the length change in isotropic nuclear graphite during irradiation at various temperatures of relatively high fluxes, while Fig. 4.3b shows the volume changes in conventional nuclear graphite during irradiation at various temperatures of relatively high fluxes.

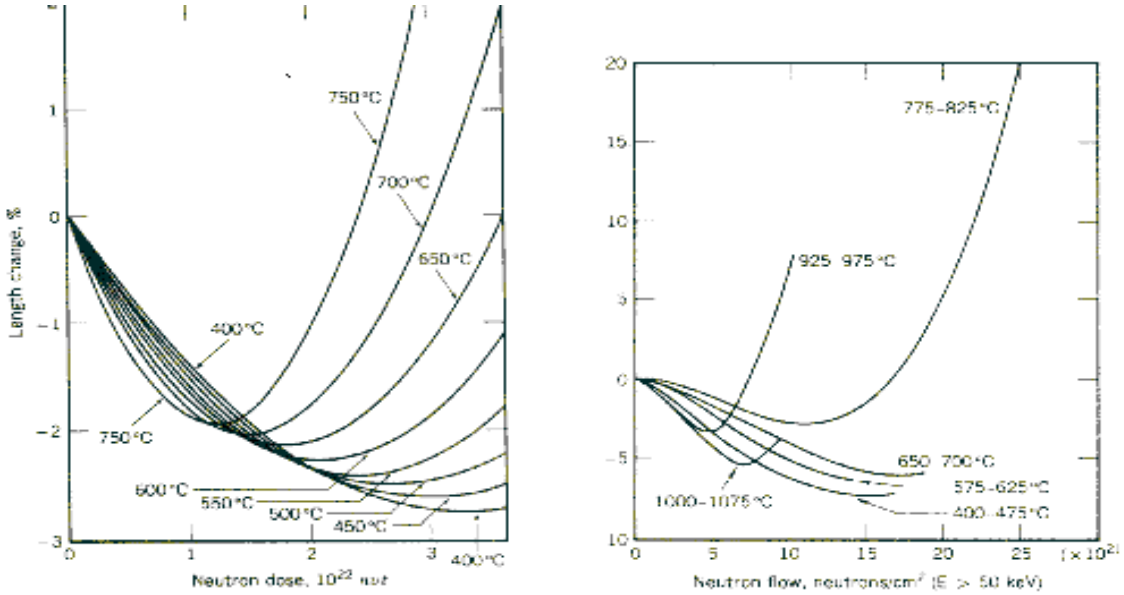

a **b**

Figure 4.3: Radiation-induced dimensional changes in isotropic graphite
(a) At various temperatures (nvt = neutron density) x velocity x time.
(b) Volume change in anisotropic graphite during General Electric Test Reactor irradiation [176].

The graphites initially contract on exposure to fast-moving neutron doses, but the rate of contraction decreases with exposure until the graphites reach a minimum volume. Further increases in neutron doses cause volume expansion, with the rate of expansion increasing very fast at a neutron dose above 3 x 10^{22} neutron/cm^2 (> 50 keV) [176].

A good moderator material must not react with neutrons, because if they are captured in the moderator, they cannot sustain the fission process. Moreover, the neutrons should slow down over short distances and there should be few collisions in the moderator. Ideally, moderators should be inexpensive and should be compatible with the reactor's structural design. A good moderator should efficiently energise fast neutrons through the process of elastic collisions. The maximum energy loss per collision occurs when the target nucleus has unit mass, and tends to zero for heavy target elements. A low atomic number is a prime requirement for a good moderator. The slow-down power should be large compared with the tendency to capture neutrons (capture cross-section), which should be small [176].

Graphite is used in nuclear reactors because of its availability, its good moderating properties and its low neutron capture cross-section of $0.0032 \pm 0.002 \times 10^{-24}$ cm^2. The latter is a factor of the purity of reactor-grade graphite, which depends on the raw material selected and on its subsequent processing and purification. The degree of purity required is determined by the reactor design. Taking into account the density of reactor-grade graphite (bulk density of 1.71 g/cm^3), the bulk neutron adsorption coefficient is 0.0003/cm. This suggests that a slow neutron may travel 32 m in the graphite without capture. The unique properties of such graphite are its mechanical strength and excellent machinability [177]. Furthermore, the thermal stability, resistance to corrosion and high thermal conductivity of graphite makes it a most suitable moderator material for consideration in advanced design, high-temperature and atomic energy-efficient nuclear reactors [177, 178].

CHAPTER 5

GRAPHITE CHARACTERISATION METHOD

Structural analysis of the graphitisable carbon produced requires instruments whose precision is necessary for reliable, accurate and reproducible results. It is important to understand the techniques used for obtaining the optical texture of the coke and the graphite, and to understand the industrial relevance of these techniques. This chapter therefore provides information on the instrumentation and operational techniques used in assessing the quality of the coke and graphite produced as discussed in the experimental section (Chapter 6).

5.1 Determination of the optical texture of the coke

The polished block of a carbon sample mounted in resin is observed using the polarised light of an optical microscope (Fig. 5.1) and an analyser at 90 °C (cross-polar). Isotropic materials such as resin appear black, whereas crystalline media reflect the light when the molecular orientation of the surface of the section is not parallel to a symmetry fold, and domains with molecules lying flat disappear (Fig. 5.2a).

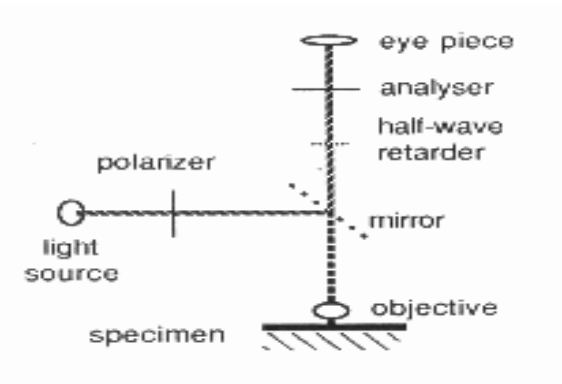

Figure 5.1: General outline of the optical microscope [178]

In other domains, disappearance occurs when molecules are parallel to either the polariser or analyser; black lines or contours are seen. The introduction of the λ-plate causes the retardation to introduce interference colours, which change with the orientation of the layers (Fig. 5.2b) [179].

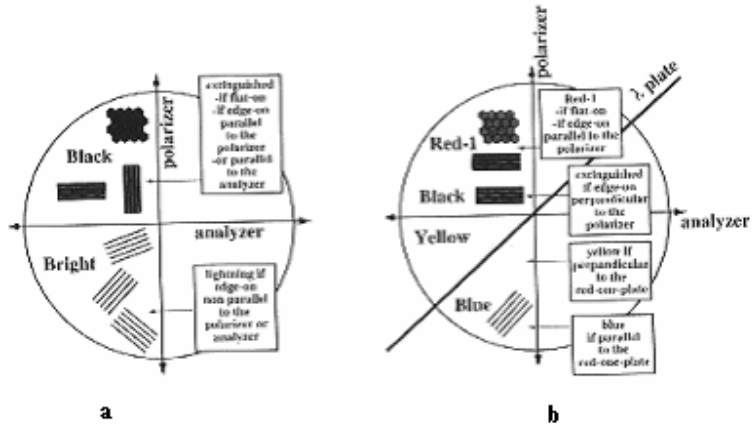

Figure 5.2: (a) Extinction and reflection under cross-polars and (b) Interference colours with the addition of a λ- plate [179]

The technique for measuring the optical anisotropy of the coke is to use a reflected polarised microscope equipped with a rotating analyser. It maps out gradients in artefacts. The reflectance of the coal macerals is used as a measure of the percentage of optical anisotropy and is a proportion of the direct light that is reflected from the polished surface under specific conditions of light exposure [179]. Vitrinite in coal develops anisotropy and thus show bi-reflectance. By measuring the true maximum and minimum reflectance, the anisotropy can be calculated by the difference R_{max} - R_{min} [179].

Consider an example illustrated with polarised optical microscopy (Fig. 5.3). The microscope is equipped with an NS polariser and a WE rotating analyser. In this example, a thick-coated fibre (~2 μm) is used. In the WE position, the rotating analyser indicates Ae = 0^{o} and the two polar hairs are said to be 'crossed' (a Maltese cross is observed).

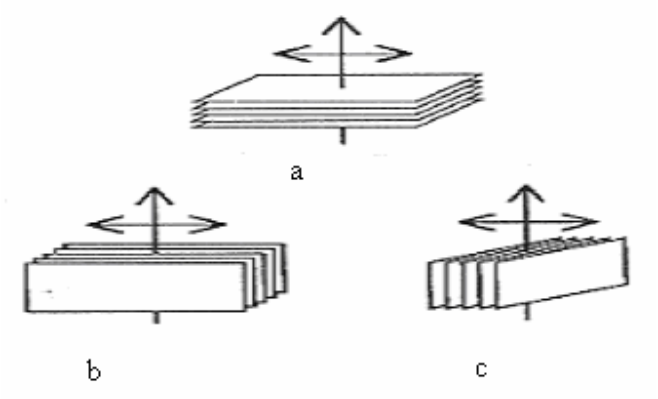

Figure 5.3: Retardation parallel plates used to observe interference colours [179]
(a) Basal plane interaction near maximum
(b) Maximum interaction with polarisation parallel to the planes
(c) Minimum interaction with polarisation perpendicular to the planes.

The measurement is made on the bisector of the first quadrant (white arrow) (Figure 5.4). The analyser is rotated clockwise so that the N and E branches of the Maltese cross fuse together on the bisectors. The quadrant is extinguished, and then becomes bright again. At the position of complete darkness, the extinction Ae is read directly on the vernier micrometer of the analyser [179]. Ae (expressed as degrees) is related to the reflectance anisotropy ratio Ro/Re by the simple relation:

$$Ro / Re = tg^2 (45 + Ae) \qquad (5.1)$$

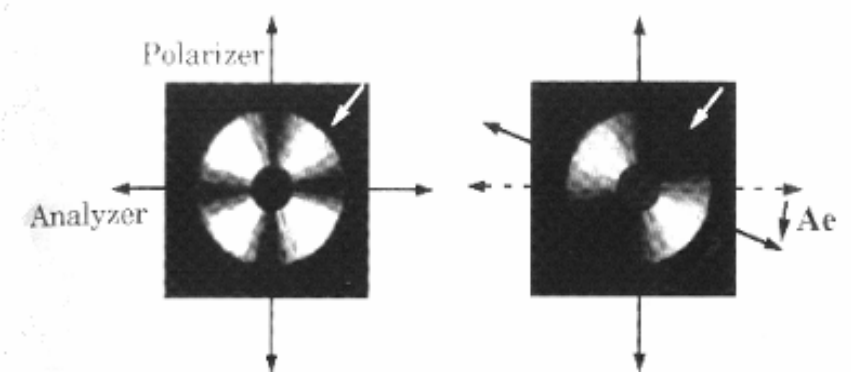

Figure 5.4: Polarised light optical microscopy showing extinction angles The extinction angle Ae is measured under cross-polarised light. The extinction is obtained in the first quadrant (white arrow) by rotating the analyser clockwise [179]

The crystallite arrangement in carbonaceous solids is observed after they have been heated to 1 000 ^{o}C. This crystallite arrangement starts over a narrow temperature range at 450 ^{o}C, coinciding with the development of the mesophase, which leads to the anisotropic structures found in coke. The shape and size of these anisotropic structures determine the behaviour of a particular coke. Unlike isotropic liquids, a crystal is characterised by a long-range order. Liquid crystals are droplets of spheres within the isotropic mass that coalesce into crystalline domains (molecular order). The molecular arrangement is envisaged as rod-shaped, with similarly sized molecules lying parallel to each other but with no stacking order. Classification of the coke is therefore based on the shape and size of the anisotropic structure, as follows [180]:

Isotropy	No optical activity, uniform, light purple colour on the surface
Anisotropy via mesophase	Dark purple, yellow and blue areas of varying shape and size
Fine-grained mosaic	Irregular shape, isochromatic areas (ISA), 0.5-1.5 µm long
Coarse-grained mosaic	ISA, 5.0 – 10 µm long
Coarse flow	Rectangular, flow-type structures, 30 -60 µm long, > 10 µm wide
Flow domains	Flow-type structures, > 60 µm long, > 10 µm wide
Domains	Isomeric structures, > 60 µm long
Basic anisotropy	Flat, featureless anisotropy associated with the parent unreacted (or slightly altered) vitrain from a high-rank coal

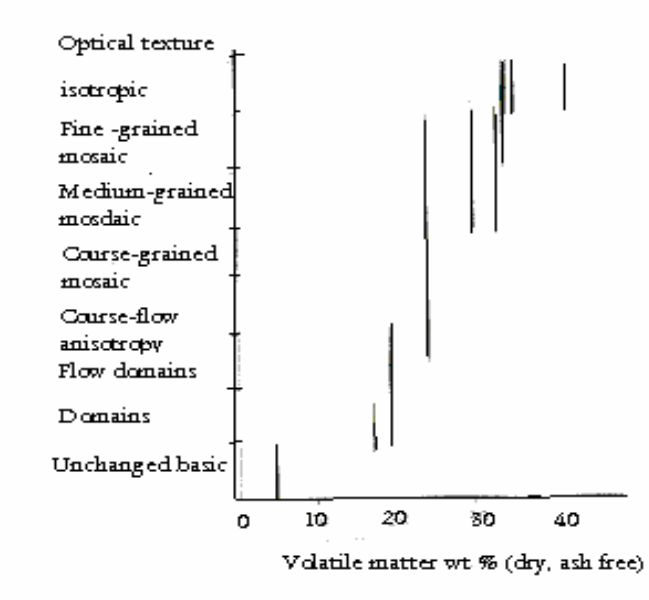

Figure 5.5: Variation of a coke's optical texture with the volatile matter content of the parent vitrains [180]

The size of the anisotropic structures in coke increases with increasing coal rank, which is a factor of the volatile matter released (Fig. 5.5) [180].

5.2 X-ray diffraction

The quantitative X-ray diffraction analysis of carbonaceous material was first conducted by Warren [93]. Today, structural parameters such as crystallite size and its distribution, L_a, L_c and d_{002}, P_n, are determined. The X-ray diffraction technique is sensitive to crystal defects, non-destructive and requires sample preparation. A high-resolution X-ray diffractometer is used with a 2.2 Kw Cu X-ray tube, the focus of which can be set to either a line or point source. For the point source, the beam is monochromised and collimated by the Ge 220 four-crystal monochromator to select the $CuK_\alpha 1$ wavelength λ (normally 0.1540511 nm) with a wavelength spread, $\Delta\lambda$, of 0.0000461 nm [181].

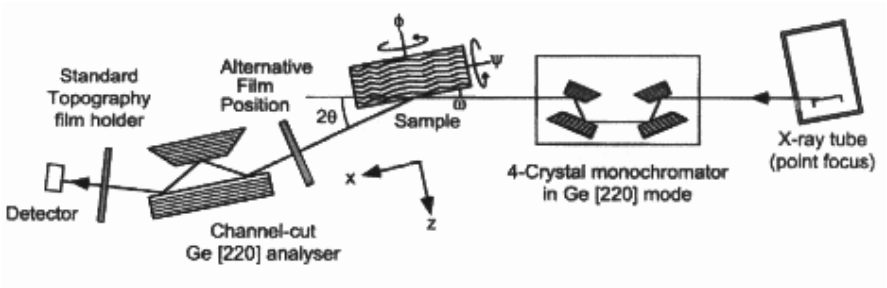

Figure 5.6: Schematic diagram of the X-ray diffraction system [181]

The incident beam is filtered by the Ge 220 monochromator. The beam reaches the sample at an angle of ω to the diffraction plane. ψ is the tilt angle of the sample and ϕ is the angle of rotation around the sample holder normally. The outcoming beam reaches the detector after having collided with the triple-axis crystal. A photographic film sensitive to X-rays can be placed before or after the triple-axis analyser crystal to produce X-ray topography images (Fig. 5.6). The

measured crystallite sizes, L_a and L_c, and the interlayer spacing, d_{002}, of the carbonised material can be obtained [181].

5.2.1 Measurement of interlayer spacing d_{002}

The interlayer spacing, d_{002}, is obtained by measuring the 2θ angle at the maximum of the 002 peak ($25^o > 2\theta < 26.6^o$ for a Cu anti-cathode). Accurate results are obtained by the addition of an internal standard (such as Si with Si_{111} at 340 pm) to a powder of the sample. The 2θ values at the maximum of the smoothed peak is used to calculate the mean d_{002}-spacing of the sample by means of the Bragg equation (5.1).

$$2d_{hkl} \sin(\theta_{hkl}) = n\lambda \qquad (5.1)$$

where θ_{hkl} is the scattering angle and d_{hkl} is the spacing between hkl planes.
The d spacing (pm and pm = 10^{-12} m) is related to the degree of graphitisation by the Maire and Meiring equation (5.2) [181]:

$$g = (3.44 - d_{(002)}) / 0.086 \qquad (5.2)$$

5.2.2 Measurement of crystallite size L_a and L_c

The coherent lengths, L_a and L_c, are estimated from the amount of peak broadening, β, using the Scherrer equation (5.3):

$$L = K\lambda / \beta\cos\theta \qquad (5.3)$$

Where L = the coherent length
λ = the wavelength
β = the width at half peak-height
θ = the Bragg angle of the line
K = the Scherrer reflection.

Measurement of the peak width, β_{002}, from the 002 or 001 reflection is used to determine the stack size, L_c.

5.3 Raman spectrophotometry

During the past few years, Raman spectroscopy has evolved as an effective technique for a rapid and non-destructive characterisation of carbonaceous materials and to follow the graphitisation process (Fig. 5.7). It relates to the frequency changes observed when a monochromatic light beam is scattered by the molecules contained in the sample. The frequency shifts observed for the scattered light are due to the interaction of the incident light with vibrating molecules [182].

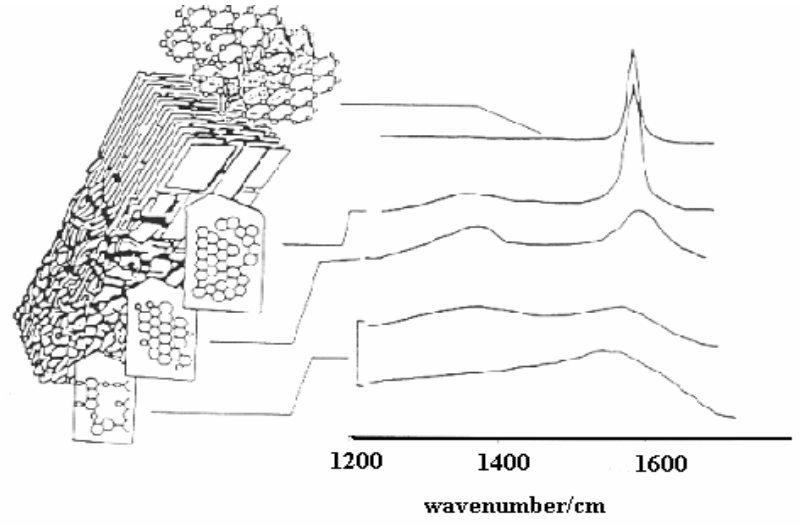

Figure 5.7: Evolution of Raman spectra from carbonaceous material to graphite [182]

5.3.1 Raman microscope

Raman microscopy is very appropriate for studying at the micrometre scale the chemical bonding, the phase composition and the crystalline state of solids, from

poorly organised to well-crystallised structures. This technique is based on the analysis of the spectral characteristics of the vibrational modes associated with the Raman shifts (wave number, bandwidth and intensity). The instrument used for this work is based on the latest fibre-bundle image compression (FIC) design, a technique that allows simultaneous collection of a spectral 3-D data cube in one read-out of a CCD detector. In this FIC-based instrument (Fig. 5.8), the light propagates from the sample to the spectrograph through an optical fibre bundle. At the collection end, the optical fibres are ordered in a square array where each fibre collects light from a unique spatial point in the sample. At the distal end of the bundle, the optical fibres are ordered in a linear stack, which serves as the entrance for an imaging spectrograph. The linear stack is attached to an imaging spectrograph and provides 80 Raman spectra per image frame, each with 900 wavelength channels.

The sample is imaged onto the fibre bundle by optically coupling the bundle to an Olympus BX-60 microscope. A x 20 microscope objective (Olympus IC-20) yields a single-frame field of view of 70 x 56 μm, with a spatial resolution of 7 μm per FIC image pixel. The sample is globally illuminated by a 500 mW diode laser (SDL-8630) operating at 785 nm, with a total power of view (or about 1 mW of excitation power per Raman spectrum). Besides the imaging capabilities of the instrument, the system can be used as a conventional Raman microscope where a single-frame field of view gives one average spectrum (single-frame exposure), corresponding to the sum of all 80 Raman spectra in a single-image frame [183, 184].

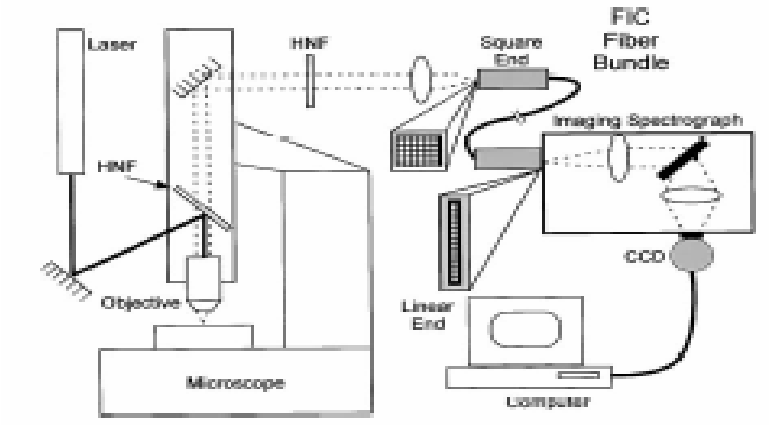

Figure 5.8: Raman imaging microscopy [184]

5.3.2 Raman spectroscopy and the optical characteristics of graphitisable carbon

Raman microscopy has been widely applied to the study of carbon materials and their graphitisation behaviour at high temperature [184]. The hexagonal graphite structure (space group D^4_{6h}) is characterised by two Raman active vibrational modes with E_{2g} symmetry (E_{2g1} and E_{2g2}). Both modes correspond to the in-plane vibrations of carbon atoms. Whereas the former mode corresponds to shear displacement of whole graphene layers (νE_{2g1} = 42 cm^{-1}, not considered here), the latter involves the stretching of the sp^2 C-C bond. Owing to the C-C covalent bond (as compared with the weak interlayer --bonding), the E_{2g2} mode (commonly referred to as the G band) is characterised by a much higher frequency (νE_{2g2} = 1 582 cm^{-1}). With disordered carbons (e.g. turbostratic), the Raman spectra commonly show an additional feature at about 1 350 cm^{-1} (D band or A_{1g} mode), as well as, in some cases, another weak band around 1 620 cm-1 (D' band), close to the G band. Both the D and D' bands are generally associated with a broadening of the G band. They are assigned to defects within the carbon microtextures (edge, distorted graphene layers, etc.) with regard to ideal graphite structure [185, 186, 187]. The 1 350cm^{-1} band is attributed to the

finite crystal size. The intensity ratio of the 1 350 cm^{-1} band to the 1 580 cm^{-1} band can be used to measure the crystal size, L_a, of the graphite sheet [122].

Structural defects have been observed in mechanically ground graphite by Raman microscopy. The interlayer spacing was found to increase during the grinding process with the reduction of the crystallite size, La, Lc. Smaller values of full width at half maximum (FWHM) of the 1 350 cm^{-1} peak in heat-treated carbon and ground carbon were observed [188].

It has been found that the lower the plasticity of the softened coal, the lower the degree of orientation of the aromatic nuclei. Inversely, the higher the plasticity of the coal, the larger the zone of anisotropy in the coke. The latter zone of anisotropy could be interpreted as a zone within the aromatic lamellae having approximately the same orientation. Higher rates of heating lead to a lower viscosity and subsequently an increased zone of anisotropy. Inversely, a sharp reduction in the rate of heating, viz. 0.5 – 1 ^{o} C/mm, can result in a higher degree of viscosity, and a reduction in the size of the zones of anisotropy and sometimes even in isotropy [189].

CHAPTER 6

EXPERIMENTAL

This chapter describes the starting material, chemicals, apparatus and experimental procedures used in obtaining the graphitisable carbon.

6.1 Chemicals used

The chemicals, all pure grade, used were: N, N-dimethylformamide (DMF) 99.9 % AR (Samsung Fine Chemicals); NaOH CP in pearl (Bio-Zone Chemicals); hydrated Na_2S 60 - 62 % (PAC Chemicals), KCN analytical grade (Rochelle Chemicals), $Na_2S_2O_3 \cdot 5H_2O$ (Acros Organics) and polyethylene glycol-400 (PGA-400). The carbon black and acetylene black, i.e. the carbon additives, were supplied by Ferro Industrial Chemicals Ltd and SA Dow (Pty) Ltd respectively. (See Appendix D.)

6.2 The solvent of choice

N-methylpyrrolidone being a relatively expensive solvent, the solvent of choice is defined by the general equation (2.5), where R_2 and R_3 = the methyl group, M = carbon, R_n = H and R_1 = 0. The structure takes the form of N, N-dimethylformamide or formic acid dimethylamide (Fig. 6.2.1), which is inexpensive and readily available in South Africa

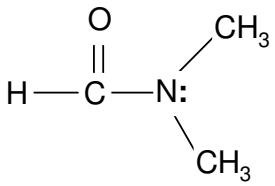

Figure 6.2.1: N, N-dimethylformamide (DMF)

N, N-dimethylformamide is a suspected carcinogen, hygroscopic and has the following physical properties (Table 4.1): density of 0.957 g/ml; Mp~ -61 ^{o}C; boiling point ~ 152 - 154 ^{o}C; flash point ~ 59 ^{o}C; viscosity/20^{o} ~8 m Pa; dipole moment/20^{o} ~ 36.7; saturation concentration/20 ^{o} ~36.7; explosive limits 2.2 - 16 vol. %; miscible with water; residue upon evaporation ≤ 0.0005 % [190, 191, 192]. The impurity levels identified include the following:

- Free acid (CH_3COOH) ≤ 0.003 %
- non-volatile matter ≤ 10 ppm
- Free alkali (NH_3) ≤ 0.005 %
- Water ≤ 0.15 %
- Residue upon evaporation ≤ 0.005 %

Table 6.2: Traces of elements present in N, N-dimethylformamide [190, 191, 192]

Element symbol	Amount mg/kg	Element symbol	Amount mg/kg	Element symbol	Amount mg/kg
Al	0.50	Cu	0.02	Ni	0.02
Ba	0.20	Fe	0.10	Pb	0.10
Bi	0.10	K	0.50	Sr	0.10
Ca	0.50	Li	0.10	Zn	0.20
Cd	0.05	Mg	0.10	Sn	0.10
Co	0.02	Mn	0.02	Mo	0.10
Cr	0.02	Na	1.00		

6.3 Coals studied

The Tshikondeni coal (ash content ~ 10 %, particle size distribution < 150 µm passing, obtained from Tshikondeni coal mine and supplied by Kumba Resources, RSA) was chosen for this research because of its availability and

solubility in dimethylformamide (DMF). Analyses of coal (air-dry basis) were done by the SABS Coal Exploration Technology Section. Table 7.1.1 gives the proximate analysis, Table 7.1.2 gives the ultimate analysis, Table 7.1.3 gives the ash analysis and Table 7.1.4 gives the petrographic characteristics of the coals.

6.4 Apparatus

This section lists the apparatus used. All electrical appliances, viz. furnaces, ovens and balances, were calibrated by Microsep Co. and Intercal Co., affiliated to the SABS's International Calibration Laboratory.

1. Outline of the reactor used in the extraction process

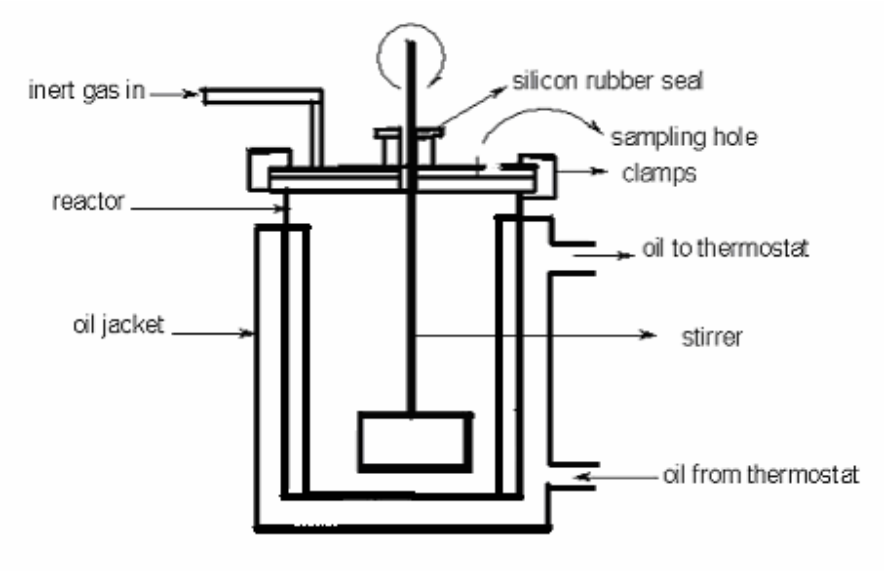

Figure 6.4.1: The reactor used for coal dissolution

2. Oven: model Labcon EFDO, supplied by Merck, equipped with an inlet for nitrogen flow which is used for drying.
3. Beckmann model GPR Centrifuge with a maximum speed of about 5 000 r/min

4. LKB Bromma 2160 Midispin Centrifuge with a maximum speed of 4 000 r/min
5. Clements GS 150 Centrifuge with a maximum speed of 2 000 r/min
6. Ohaus Explorer balance, 2 100 g full-scale capacity with a resolution of 0.001 g.
7. Mixer: Ultra-TURRAX TIZ5, IKA-Labortech, max. speed 2 400 r/min
8. Stirrer: Heilddph-Labortech, 140 – 1 100 r/min
9. Furnace system (used in pyrolysis): supplied by Prestige Furnace and Engineering, with nitrogen blanketing and automated temperature programmer important in carbonisation (Fig. 6.4.2).

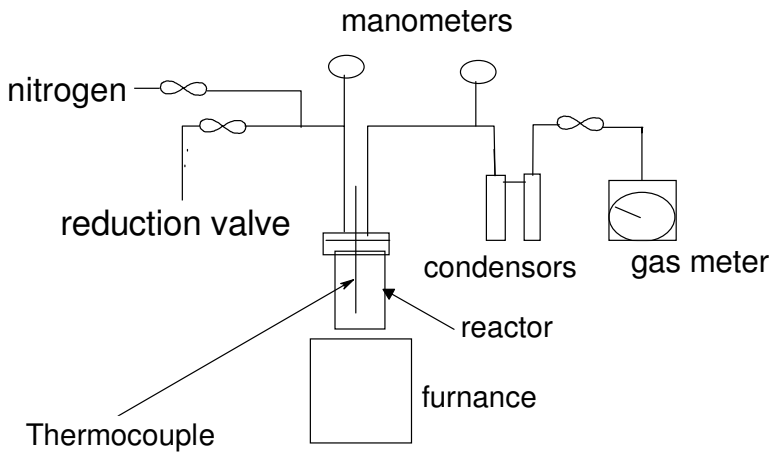

Figure 6.4.2: Furnace system used for pyrolysis

6.5 Instruments used to analyse the results

The instruments described in this section were used in the analysis of the results. In each case, the method of analysis is also described.

6.5.1 Spectronic Genesis - 5 Ultra-Violet Spectrophotometer

This instrument was used to measure the degree of extraction by measuring the optical transmission of the diluted samples at 600 nm.

6.5.2 Optical microscopy

To obtain optical micrographs and reflectance, an optical microscope equipped with a computerised digital camera (Olympus DP B10 with soft imaging system) was used to observe the surface characteristics of the coke (courtesy of the Department of Geology University of Pretoria). Reflectance measurements were taken on each of the samples in accordance with the ISO Standards 7404-5 of 1994 by the Petrology Section of Coal and Mineral Technologies (Pty) Ltd at the SABS. An assessment of the microscopically recognisable coke textural characteristics was made with reference to the AS Standards D 5061-92 (courtesy of the SABS, Coal and Mineral Technologies (Pty) Ltd). For each set of two measurements, the object stage was turned through an angle of 90 ^{o}C and the maximum and minimum reflectance values recorded.

In order to view the samples under an optical microscope, it is necessary to prepare a highly reflecting, polished surface. To facilitate the polishing of the very brittle samples, a cross-section of each sample was mounted in Bakelite resin. In order to expose the sample and prepare a flat surface, the initial grinding was carried out on a grinding disc fitted with 120, 600 and 1 200 grades of diamond disc, over which water was flowing continuously. Grinding was carried out on the successively fine grades until a flat, even surface ready for polishing was obtained.

Polishing was done using successive grades of diamond pastes (9, 6, 3 and 1 microns), starting with the coarsest and finishing with the very fine grade. A rotating lap was used for the final polishing using the diamond paste. The laps

were covered with cloth (Poly Pan 2) and water continuously dripped on the cloth. When polishing was considered to be satisfactory, the samples were mounted on a glass slide with plasticine using a hand mounting press to enhance evenness. The polished surface was protected from abrasion during the mounting by a soft tissue. Samples of the cokes produced were examined under polarised light in a reflectance optical microscope. The samples were then placed on the rotating stage of the microscope (Standard Universal-Carl Zeiss) and examined by reflected polarised with an Antiflex-epi Zeiss objective lens (Figs 7.2.14 to 7.2.17, courtesy of the SABS). The optical micrographs shown in Figs 7.3.9, 7.3.10, 7.3.16, 7.3.17, 7.4.1 and 7.4.2 were taken with a digital Olympus camera.

6.5.3 Thermogravimetry

The thermogravimetric analyser (Mettler Toledo TGA/SDTA 851^e thermal analyser) was equipped with an additional sensor to record the temperature difference between the temperature measured directly at the sample and the model reference temperature. Thermogravimetric analysis monitors the weight losses as the temperature is increased [187]. Weight losses occur as a result of water and the other volatiles being driven off. About 10 mg of sample was placed in aluminium crucibles, 70 µl capacity, and heated in a thermo balance at the rate of 10 $^oC\ min^{-1}$ to 900 ^oC, in a nitrogen flow of 50 ml/min. The weight loss of each sample as a function of temperature is shown in Figs 7.3.4, 7.3.5, 7.3.6, 7.3.7 and 7.3.8.

6.5.4 X-ray diffraction analysis

The series of graphite samples, about 2.0 g each, were ground together with about 0.150 - 0.20 g of silicon (99.9% Merck with crystallite sizes up to 45 µm to pass through a 240 BSS mesh sieve). About 0.6 g (16 drops of PEG) and 1 to 2 ml of ethanol as a wetting agent were added to the mixture. After thorough

mixing, the ethanol was evaporated. The ground sample was placed in a 0.3 mm silica glass capillary and an X-ray powder photograph was taken using a 57.4 mm camera fitted to a Phillips PW 1010/30 X-ray diffraction unit operating with filtered CuKα radiation.

The X-ray line profiles were plotted out on graph paper and the width of the (002) and the adjacent silicon peak determined at half the peak intensity. The instrument broadening and the broadening due to small crystalline sizes were merely additive. The peak intensity and the crystalline sizes (L_c) determined from the corrected broadening (β) were calculated and the results are shown in Tables 7.2.7, 7.3.2 and 7.4.1 and Figs 7.2.19, 7.3.14. 7.3.15, 7.4.3 and 7.4.4.

6.5.5 Raman spectroscopy

Raman spectra were recorded with an XY Raman spectrometer from Dilor®, using the λ = 514.5 nm laser line of a Coherent Innova®90 $Ar^{\pm}$ laser, with a resolution of at least 2 cm^{-1}. The samples were recorded in a backscattering configuration under the microscope attached to the instrument, using a 50 x microscope objective. The presence of the confocal pinhole before the spectrometer entrance ensures a sampling of 1 - 3 µm diameter area using the objective, with the final laser power of about 1-4 mW at the sample surface. Acquisition time is about 20 – 300 s and 15 - 20 spectra are recorded for each sample. A liquid-nitrogen-cooled CCD detector was used with the laser power 200 mW at the laser exit, resulting in a laser power of < 20 mW at the sample. The spectra were baseline corrected, using the Labspec software program supplied by Dilor®. Raman microscopy was performed on the graphitised samples. The Raman spectra of the graphites are depicted in Figs 7.2.20, 7.2.21, 7.3.11, 7.3.12, 7.3.13, 7.4.1 and 7.4.6 and in Tables 7.2.7, 7.3.2 and 7.4.1.

6.5.6 Scanning electron microscopy (SEM)

Images and identification of some phases of the coal extracts samples were obtained on a JEOL JSM-6300 Scanning Microscope. SEM photomicrographs are shown in Figs 7.3.1, 7.3.2 and 7.3.3.

6.6 Experimental procedures

This section describes the procedures used in obtaining the data.

6.6.1 Measurement of the degree of extraction

A 0.7 litre reactor of stainless steel tubes equipped with a lid, fitted with a small metal stirring plug and operated at room temperature, was charged with coal (7 g), fresh DMF (70 g), NaOH (0.7 g), and different amounts of the nucleophile (A^{-1}) with NaOH:A^- (where A^- is S^{-2}, CN^{-1}, and $S_2O_3^{-2}$) mole ratios of 4:1, 2:1 and 1:1, and tumbled end to end for 24 h. The solution was then centrifuged and filtered using a pre-weighed sintered glass funnel. The residues were washed five times with fresh DMF, centrifuged (LKB Bromma 2160 Midispin Centrifuge, speed 5 000 r/min) and the supernatant decanted. Thereafter, the residues were washed with deionised water and filtered in the pre-weighed sintered glass. They were then dried to constant weight in an oven at 60 ^oC, weighed, and analysed for C,H,N,S. The degree of extraction was calculated as follows:

$$\% \text{ Carbon extraction} = \frac{W_t \text{ of carbon in coal} - W_t \text{ of carbon in residue}}{W_t \text{ of carbon in coal}} \times 100$$

The results are shown in Tables 7.2.4, 7.2.5 and 7.2.6 (data obtained from Appendix A1) and Figs 7.2.10 and 7.2.11.

6.6.2 The scaled-up extraction process

To a 1-litre reactor equipped with a hot water or oil jacket (Fig. 6.4.1) (Jalabo MD, Laborteck) and operated at temperature of 90 ± 2 ^{o}C, 80 g of coal was charged together with 800 g of fresh DMF. The mixture was stirred at 700 r/min (Heilddph Labortech stirrer, 140 – 1 100 r/min) and allowed to reach operating temperature. At that operating temperature, 8 g of sodium hydroxide (in pearl form) was added. To maintain an absolutely inert environment within the reactor, a slow stream of nitrogen was flushed into the dissolver to maintain a slight positive pressure. A near-perfect seal of the reactor was effected by means of silicone rubber tubing around the stirrer shaft. The extraction period was 4 – 5 min. The inorganic mineral components and undissolved coal were separated by centrifugation (Beckman GPR Centrifuge, speed 5 000 r/min) for 1 h.

6.6.3 Monitoring the progress of extraction

Samples of about 2 ml of the slurry in the reactor were taken at regular suitable intervals. The samples were centrifuged (Clements GS 150 Centrifuge, maximum speed of 4 000 r/min) for 4 min. About 0.1 g of the supernatant solution was weighed into a 50 ml volumetric flask and made up to the mark with fresh DMF. The absorbance at 600 nm was read on a Spectronic Genesis - 5 UV Spectrophotometer. The nitrogen-purged coal solution was then tightly sealed and centrifuged at 3 000 r/min for 1 h to separate the ash and insoluble organics from the coal solution. The decanted coal extract solution was then immediately used in the recovery process. (See Section 6.5.4). The reproducibility of different separate extraction runs is shown in Fig. 7.2.1. The various curves showing the progress of extraction are given in Figs 7.2.2, 7.2.3, 7.2.4 and 7.2.6. The extraction properties of the coal extract solution are shown in Figs 7.2.5 and 7.2.7 and in Table 7.2.1.

6.6.4 Recovery of the coal extracts from the solution

To a 1-litre Teflon bottle containing deionised hot water (60 °C, 100 g), purged with nitrogen for 10 min, about 400 g of the Refcoal solution (constant ratio of 1:2) obtained as described in Section 6.6.2 was added and thoroughly mixed. The mixture was then centrifuged (4 000 r/min for 30 min). The gel obtained after decantation of the supernatant solution was thoroughly washed with deoxygenated water (process repeated x 4), filtered (Buchner funnel) under nitrogen, and dried overnight in a slow stream of nitrogen at 60 °C. The washing efficiency calculated from equation 6.1 was kept consistent at 33 %. The characteristics of the coal extract are shown in Tables 7.2.2, 7.2.3, 7.2.4, 7.2.5, 7.2.6 and 7.3.1 and in Figs 7.2.7 and 7.2.8.

$$WashingEfficiency = \left(\frac{M_{gel}}{M_{gel} + M_{supernatant}} \right)^{n} \qquad (6.1)$$

Where

M_{gel} = mass of the coal extract gel

$M_{supernatant}$ = mass of the decanted supernatant solution.

N = number of washings

6.6.5 Dissolution of coal into DMF, with NaOH and Na_2S

The same procedure described in Section 6.6.2, but with the addition S^{-2}, was followed. The reactor was charged with coal (80 g), fresh DMF (800 g), NaOH (8 g) and different amounts of sodium sulphide in separate extraction runs, and each was stirred for 6 to 7 h. The molar ratios of NaOH: Na_2S were 4:1, 2:1 and 1:1. Following the monitoring and recovery procedures, described in Sections 6.6.3 and 6.6.4 respectively, the coal extracts and their blend of sodium sulphide were carbonised using the method described in Section 6.6.6. The results with

regard to the behaviour of the coal extracts are shown in Tables 7.2.1 and 7.2.3, and the elemental analysis is given in Table 7.3.1.

The plastic properties of the coal extracts obtained were measured in accordance with SABS Method 933 by Kumba Resources laboratories using a constant–torque Gieseler plastometer. Samples of the coal extracts were sent to the SABS (Coal and Mineral Technologies laboratory) for measurement of the swelling index. The Gieseler fluidity test measures the rotary speed (in dial divisions per minute, ddpm) of a stirrer under a constant torque in a compacted 5-g charge, heated at 30 ^{o}C/min from 300 ^{o}C until it resolidifies (Table 7.2.3.)

6.6.6 Dissolution of coal at room temperature

To a 1-litre Teflon bottle charged with coal (80 g), fresh DMF (800 g) and NaOH (8 g), and purged with nitrogen for 10 min, sodium sulphide of molar ratios (NaOH:Na_2S) 4:1, 2:1 and 1:1 were separately added and continuously stirred at 600 r/min over a magnetic stirrer for 72 h. The same procedure was then followed again, but without the addition of sodium sulphide. The mixtures were each charged separately into the reactor. The procedure described in Section 6.6.4 was then followed to recover the organic solids. The results obtained are shown in Fig. 7.2.9.

6.6.7 Carbonisation of the coal extracts

The coal extracts were carbonised by step heating in a nitrogen atmosphere to 480 ^{o}C at a rate of 10 ^{o}C min^{-1} and held at the maximum temperature for 1 h, then heated to 900 ^{o}C at the same rate and held for 2 h. The flow diagram of the furnace used in the pyrolysis is shown in Fig. 6.4.2. The samples were weighed before and after pyrolysis, and the percentages of weight loss or volatiles are shown in Figs 7.2.13 and 7.2.18. The process of mounting the resultant cokes in a thermosetting resin for sectioning and polishing is described in Section 6.5.2.

The optical textures of the cokes were characterised in terms of the size and domain texture of the observed areas. The optical micrographs of the cokes are shown in Section 6.5.2.

6.7 Control of the flow texture of the coke obtained from pyrolysis of the S^{-2} derived coal extracts

To a 500 ml Teflon bottle, about 0.044 g, 0.088 g and 0.160 g each of the carbon additive corresponding to 76 % carbon in the coke was added into 200 g of the prepared coal extract solutions at room temperature. The additive was dispersed by a high-shear mixer (Turrax TIZ5 mixer, max. speed 2 400 r/min) into the coal extract solution for 10 min. During mixing, a continuous flow of nitrogen was purged into the mixture and additional stirring allowed over a magnetic plate. The dispersed carbon additive was observed through a transmission electron microscope (Figs 7.3.1, 7.3.2 and 7.3.3). Recovery of the organic extract solids was achieved by mixing a definite proportion of the coal extracts with deionised hot water (~ 60 ^{o}C), purged with nitrogen (see Section 6.6.4). The precipitates were thoroughly washed, then filtered under nitrogen. The process was repeated four times with a consistent washing efficiency of 33 % (calculated from equation 6.1). The resulting cake was dried overnight at 60 ^{o}C under nitrogen. The chemical composition of the dry coal extracts (C, H, S, N and O by difference) determined is given in Table 7.3.1. The dry coal extracts were then carbonised as described in Section 6.6.7. The carbon yield (CY) was obtained from the weight difference of the carbon substrate and corrected for the amount of carbon additives added. The cokes produced were evaluated in terms of the optical texture of the polished surface. The results of the weight loss (%) and optical texture are given in Figs 7.3.4, 7.3.5, 7.3.6, 7.3.7 and 7.3.8, and in Figs 7.3.9 and 7.3.10 respectively.

6.8 Addition of carbon black and iron (III) to the coal extract solution prepared at room temperature without the addition of sodium sulphide

The coal extracts without S^{-2} were prepared as described in Section 6.6.6 in a 1-litre Teflon bottle. Small amounts of about 0.015 g, 0.022 g and 0.044 g each of the carbon black, corresponding to about 75 % carbon in the coke, were added into 200 g of the coal extract solution. The mixture was stirred with a high-shear mixer (Turrax TIZ5 mixer, max. speed 2 400 r/min) under nitrogen for 10 min and over a magnetic stirrer. The organic solids were recovered as described in Section 6.6.4 and coked using the method described in Section 6.6.6. Similarly, using prepared room-temperature coal extract solution, small amounts of about 0.01 g and 0.03 g of iron (III) gel were mixed into 200 g portions of the solution and the resin-mounted polished cokes were observed under an optical microscope. The graphitised cokes at 2 950 ^{o}C were characterised by Raman microscopy and X-ray diffraction spectrometry.

6.9 Graphitisation

Samples of cokes were graphitised by means of a Thermtron at 3000 ^{o}C under a total nitrogen flow of 17 kg/h for 2, 3 and 6 h, in a Plasma furnace (Plasma burner 80 kW, 150 kW DC, water-cooled resistor 0.28 Ω). The graphitised cokes were assessed by means of Raman spectroscopy and X-ray diffraction. The behaviour of the graphitised cokes and their blends of carbon additives was characterised in terms of percentage weight loss and the results are given in Fig. 7.3.18. The micro-textures of the graphites are given in Figs 7.3.16 and 7.3.17.